Three-Neutrino Analysis of the Super-Kamiokande Solar Neutrino Data

C.E.C. Lima [a,1], H.M. Portella [b,2] and L.C.S. de Oliveira [a,3]

[a] *Centro Brasileiro de Pesquisas Físicas, Rua Dr. Xavier Sigaud 150, Rio de Janeiro, RJ, 22290-180, Brazil*

[b] *Universidade Federal Fluminense, Av. Litorânea s/n, Niterói, RJ, 24210-340, Brazil*

Abstract

We apply three neutrino oscillations in vacuum to explain the Super-Kamiokande solar neutrino data, considering the yearly averaged seasonal variation and recoil-electron spectrum. We show that the range 3.65 x $10^{-11} \leq \delta^2_{m_{21}} \leq$ 1.45 x 10^{-10} eV^2 and 3.25 x $10^{-4} \leq \delta^2_{m_{31}} \leq$ 1.45 x 10^{-3} eV^2 for the mass parameters are sufficient to explain the data. We also demonstrate that our mixing angle and mass regions are consistent with the CHOOZ experiment constraints and that for the neutrino oscillations in vacuum it is necessary three-neutrino flavours to explain the solar neutrino problem.

Keywords: Super-Kamiokande, solar neutrinos, neutrino oscillations.

PACS: 14.60.Pq, 26.65.+t, 13.15.+g

[1] ceclima@cbpf.br
[2] hmport@if.uff.br
[3] oliveira@cbpf.br

1 Introduction

The Super-Kamiokande detector is a large tank filled with 50 Ktons of purified water with the inner wall covered by 11000 photomultiplier tubes collecting the Cherenkov light produced in the neutrino-electron collisions. Super-Kamiokande is sensitive not only to the $\nu_e + e^-$ scattering but also to the $(\nu_\mu, \nu_\tau) + e^-$ scatterings. This detector is able to obtain data from solar and atmospheric neutrinos, but in this work we will attain ourselves to the former.

Since 1996, the Super-Kamiokande Collaboration has accumulated data from the ^{8}B solar neutrino flux. This data acquisition has indicated an excess of events for energies higher than 13 MeV, but it has been reduced (about 33%) from the 504 [1] and 708 [2,3] days to the 825 [4] and the recent 1117 [5] days data, which lead us to think in a low statistical origin for this excess disfavouring, but not neglecting yet, the hypothesis of a Hep neutrino flux larger than the calculated in the BBP98 SSM [6]. Usually the Hep neutrino source is not considered in the calculation of the suppression rates because it accounts for less than 1% of the SSM flux although it lies in the same energy region of the ^{8}B flux, but some authors [7,8] suggest that a Hep neutrino flux 20 times larger than the calculated in the BBP98 SSM could explain this excess.

In our study we first determine the limits for $\delta^2_{\mathrm{m}_{21}}$ and $\delta^2_{\mathrm{m}_{31}}$ that will constrain our analysis, as shown in section 2. In section 3, we show how to calculate the suppression rates with the inclusion of the recoil-electron spectrum. We calculate the allowed regions for the parameters $\delta^2_{\mathrm{m}_{21}}$, $\delta^2_{\mathrm{m}_{31}}$, $\sin^2(2\omega)$ and $\sin^2(2\phi)$. We made the calculation with the one year averaged seasonal variation [9], taking into account the recoil-electron spectrum and integrating over 18 energy bins in the range from 5.5 to 20.0 MeV, corresponding to the data points given in ref. [5]. In our study we do not use the low energy data with energy about 5.0 MeV, because its systematic error is under study by the Super-Kamiokande Collaboration. In section 4, we demonstrate that the χ^2 analysis finds a global and a local best fit point which are compared with the 1117 days data, and we show that our values for the mixing angles and masses are in agreement with the allowed regions from the CHOOZ experiment [10]. We also calculate the seasonal suppression rate variation, for 8 time bins of 1.5 months for the neutrino energy greater than 11.5 MeV [4,5]. The evidence of the existence of vacuum oscillations comes from the observation of the seasonal effect, although the recent Super-Kamiokande solar neutrino data are in good agreement with the expected seasonal variation in absence of oscillations, due to the eccentricity of the Earth orbit only, future experiments as the Borexino [11] and KamLAND [12], which will be sensitive to the ^{7}Be line source neutrinos can give decisive conclusions about the seasonal effect and vacuum oscillations. In section 5 we comment our results and give the conclusions.

2 Estimative of the Parameters $\delta^2_{\mathrm{m}21}$ and $\delta^2_{\mathrm{m}31}$

Before the calculation of the suppression rates we have to make some considerations about the limits for the mass parameters, $\delta^2_{\mathrm{m}21}$ and $\delta^2_{\mathrm{m}31}$, which will be used in this work. These choice of limits will deeply constrain our analysis.

In the three-neutrino scenario, the ν_e survival probability, for vacuum oscillations is given by [13]:

$$\begin{aligned} P_{\nu_e\nu_e}(\mathrm{t},\mathrm{E}_\nu) = 1 &- \cos^4(\phi)\sin^2(2\omega)\sin^2(\frac{\delta \mathrm{m}^2_{21}\mathrm{X}_{21}(\mathrm{t})}{4\hbar \mathrm{c}\mathrm{E}}) - \\ &- \cos^2(\omega)\sin^2(2\phi)\sin^2(\frac{\delta \mathrm{m}^2_{31}\mathrm{X}_{31}(\mathrm{t})}{4\hbar \mathrm{c}\mathrm{E}}) - \\ &- \sin^2(\omega)\sin^2(2\phi)\sin^2(\frac{\delta \mathrm{m}^2_{32}\mathrm{X}_{32}(\mathrm{t})}{4\hbar \mathrm{c}\mathrm{E}}) \end{aligned} \tag{1}$$

where ω and ϕ are the $\nu_{e,\mu}$ and $\nu_{e,\tau}$ mixing angles, respectively, $\delta^2_{\mathrm{m}21}$, $\delta^2_{\mathrm{m}31}$ and $\delta^2_{\mathrm{m}32}$ are the difference of the squared masses of the eigenstates ν_1, ν_2 and ν_3 and $\mathrm{X}_{21}(\mathrm{t})$, $\mathrm{X}_{31}(\mathrm{t})$ and $\mathrm{X}_{32}(\mathrm{t})$ are the distances crossed by each state which are sensitive to the seasonal variation effect. The essential point introduced in this work is that in our study we assume different lenghts for each mass combination scheme, considering much more oscillations for the "heavy" states $\delta^2_{\mathrm{m}32}$ and $\delta^2_{\mathrm{m}31}$ than for $\delta^2_{\mathrm{m}21}$.

Considering a mass hierarchy where $\mathrm{m}_1 << \mathrm{m}_2 << \mathrm{m}_3$ [14], we can verify that $\delta^2_{\mathrm{m}32} \approx \delta^2_{\mathrm{m}31}$ enabling us to simplify the equation (1) to:

$$\begin{aligned} P_{\nu_e\nu_e}(\mathrm{t},\mathrm{E}_\nu) = 1 &- \cos^4(\phi)\sin^2(2\omega)\sin^2(\frac{\delta \mathrm{m}^2_{21}\mathrm{X}_{21}(\mathrm{t})}{4\hbar \mathrm{c}\mathrm{E}}) - \\ &- \sin^2(2\phi)\sin^2(\frac{\delta \mathrm{m}^2_{31}\mathrm{X}_{31}(\mathrm{t})}{4\hbar \mathrm{c}\mathrm{E}}) \cdot \end{aligned} \tag{2}$$

The parameter $\delta^2_{\mathrm{m}32}$ is very important for the muon neutrino survival probability, in the case of the atmospheric neutrino where the $\nu_\mu \overrightarrow{\leftarrow} \nu_\tau$ oscillations are predominant. But, here we are dealing with $\nu_e \overrightarrow{\leftarrow} \nu_\tau$ oscillations and in order to maintain an equivalence to both cases we must choose for X_{31} a distance compatible with the one crossed by the atmospheric neutrinos. Notice that if we maintain the distance X_{31} the same as X_{21} and choose $\delta^2_{\mathrm{m}31}$ in the range 10^{-3} to 10^{-2} eV^2, concerning to the atmospheric neutrinos, the argument in $\sin^2(\frac{\delta \mathrm{m}^2_{31}\mathrm{X}_{31}(\mathrm{t})}{4\hbar \mathrm{c}\mathrm{E}})$ becomes huge, creating thus a possibility of averaging this term to $\frac{1}{2}$ leading to a "non-dependence" in $\delta^2_{\mathrm{m}31}$. However, with our choice of $\mathrm{X}_{31}(\mathrm{t})$ this does not occurs and the mass parameter $\delta^2_{\mathrm{m}31}$ remains very important. In a

first approximation we will consider only downward neutrinos, giving a range for X_{31} from 1.0 x 10^4 to 4.0 x 10^4 m. This choice of limits maintain an equivalence with the atmospheric neutrino production height [15].

As the minimum and maximum values for $\sin^2(\frac{\delta m^2_{31} X_{31}(t)}{4\hbar cE})$ are 0 and 1, it is easy to find the range for $\delta^2_{m_{31}}$, with the defined limits of X_{31} for the Super-Kamiokande event energies from 5.5 to 20.0 MeV.

Thus, we get the following expression

$$\delta m^2_{31} = (n + \frac{1}{2})\pi \frac{4\hbar cE}{X_{31}} \cdot \tag{3}$$

It is not necessary to calculate the parameter δm^2_{31} for many values of n, because it will give the same values for $\sin^2(\frac{\delta m^2_{31} X_{31}(t)}{4\hbar cE})$, thus using n=0 and 1 in eq.(3) we obtain the estimated limit for $\delta^2_{m_{31}}$

$$1.71 \text{ x } 10^{-4} \leq \delta^2_{m_{31}} \leq 7.45 \text{ x } 10^{-3} \text{ eV}^2. \tag{4}$$

In the computation of the suppression rates, to be made on next section, we will fix the mean value of X_{31} in 1.49 x 10^4 m. This choice is totally arbitrary and was made in order to maintain a proportion with the $\nu_e \overrightarrow{\leftarrow} \nu_\mu$ oscillation lenght, but other values in the limits of X_{31} given above can be used.

The same procedure is adopted to find the limits for $\delta^2_{m_{21}}$. In this case we find

$$1.47 \text{ x } 10^{11} \leq X_{21} \leq 1.52 \text{ x } 10^{11} \text{ m} \tag{5}$$

because $X = X_0\,(1 \pm \xi)$, for the perihelium and aphelium, with $X_0 = 1.49$ x 10^{11} m, the mean Sun-Earth distance and the orbit eccentricity (ξ) of about 0.0167. In this way $\delta^2_{m_{21}}$ lies in the range

$$1.35 \text{ x } 10^{-11} \leq \delta^2_{m_{21}} \leq 5.07 \text{ x } 10^{-10} \text{ eV}^2. \tag{6}$$

Thus in the next section we will constrain our analysis to these limits for the mass parameters.

3 Calculation of the Suppression Rates

In the calculation of the suppression rates for the Super-Kamiokande detector we take into account the recoil-electron energy spectrum and divide it into 18 bins with 0.5 MeV, starting with 5.5 MeV, but the last bin is integrated in the limit 14.0 to 20.0 MeV. This covers the 18 experimental data points. The theoretical suppression rate is given by the formula below, where we divide

the expected signal using neutrino oscillation in the SSM [6] by that one in the absence of oscillations.

$$R_i^{\rm Theo} = \frac{S_i^{\rm Osc}}{S_i^{\rm SSM}} \tag{7}$$

with

$$S_i^{\rm Osc} = \Phi_{^8{\rm B}} \int_{{\rm E}_i^{\rm min}}^{{\rm E}_i^{\rm max}} {\rm dE}_\nu \eta({\rm E}_\nu) \int_{{\rm T}_{\rm min}-{\rm m_e}}^{{\rm T}_{\rm max}-{\rm m_e}} {\rm dT} \int_0^{{\rm T'}_{\rm max}} {\rm dT'} \epsilon({\rm T'},{\rm T}) \cdot$$
$$\cdot \left\{ \langle P_{\nu_e\nu_e}({\rm E}_\nu)\rangle \frac{{\rm d}\sigma_{\nu_e}({\rm T'},{\rm E}_\nu)}{{\rm dT'}} + (1 - \langle P_{\nu_e\nu_e}({\rm E}_\nu)\rangle) \frac{{\rm d}\sigma_{\nu_\mu}({\rm T'},{\rm E}_\nu)}{{\rm dT'}} \right\} \tag{8}$$

and

$$S_i^{\rm SSM} = \Phi_{^8{\rm B}} \int_{{\rm E}_i^{\rm min}}^{{\rm E}_i^{\rm max}} {\rm dE}_\nu \eta({\rm E}_\nu) \int_{{\rm T}_{\rm min}-{\rm m_e}}^{{\rm T}_{\rm max}-{\rm m_e}} {\rm dT} \int_0^{{\rm T'}_{\rm max}} {\rm dT'} \epsilon({\rm T'},{\rm T}) \frac{{\rm d}\sigma_{\nu_e}({\rm T'},{\rm E}_\nu)}{{\rm dT'}} \tag{9}$$

where Φ is the total ^{8}B neutrino flux, $\eta({\rm E}_\nu)$ is the normalized neutrino energy spectrum, $\frac{{\rm d}\sigma_{\nu_\alpha}({\rm T'},{\rm E}_\nu)}{{\rm dT'}}$ is the differential detection cross section for the type $\alpha = e, \mu$ neutrino.

In our study we are not considering possible effects due to CP violation, so we can assume that $P_{\nu_\alpha\nu_\beta} = P_{\nu_\beta\nu_\alpha}$ and from the CPT invariance we have $P_{\bar{\nu}_\alpha\bar{\nu}_\beta} = P_{\nu_\beta\nu_\alpha}$ [16] with α,β = e,μ or τ.

The energy resolution $\epsilon({\rm T'},{\rm T})$ is described by

$$\epsilon({\rm T'},{\rm T}) = \frac{1}{\sqrt{2\pi}\Delta_{\rm T'}} \exp\left\{ -\frac{({\rm T'} - {\rm T} + \delta)^2}{2\Delta_{\rm T'}^2} \right\} \tag{10}$$

where T and T' are the measured and true electron kinetic energy, respectively, and the limit T'$_{\rm max}$ in the third integral of the eqs.(8) and(9) is the maximum kinetic energy that an electron can achieve given the neutrino energy E$_\nu$. T'$_{\rm max}$ = E$_\nu$/(1 + m$_e$/2E$_\nu$) and δ is the uncertainty in the absolute energy calibration which for Super-Kamiokande is $\pm$ 100 KeV. For more details see [17]. Our χ^2 analysis, for the recoil-electron spectrum, follows the prescriptions adopted by M.C. Gonzales-Garcia et al. [18].

4 Analysis of the Results

In figure 1 we present six projections in the phase spaces that represent the four parameters, δm^2_{21},δm^2_{31}, $\sin^2(2\omega)$ and $\sin^2(2\phi)$, which rules our analysis. From figure 1(a) we see that the limits for these mass parameters are in good agreement with the estimated values made in section 2 and we found indeed a range for them even smaller than the expected.

For the 18 energy bins of the 1117 days data we have not found solutions with only two neutrino generations, since at 99% C.L. we obtained the minimum values 0.25 for $\sin^2(2\omega)$ and 0.16 for $\sin^2(2\phi)$ and we only obtained maximal mixing for $\sin^2(2\omega)$, that is related to $\nu_e \rightleftarrows \nu_\mu$ oscillations, with 99% C.L.. The maximum value for $\sin^2(2\phi)$ with the same precision was 0.95. These values for the mixing angles imposes the need of a three-neutrino scenario to explain the Super-Kamiokande data for neutrino oscillations in vacuum. We can also remark that solutions with $\sin^2(2\phi)$ around 0.50 are excluded, as seen in the figure 1(f) where we ploted $\sin^2(2\omega)$ X $\sin^2(2\phi)$. The limits for the mass parameters and mixing angles are shown in table 1, for 90%, 95% and 99% C.L..

The plot δm^2_{31} X $\sin^2(2\phi)$ ilustrated in figure 1(e) are compared with the CHOOZ Collaboration results, as seen from figure 2. In this figure we can observe that only a small region with 99% and 95% C.L. lies in the CHOOZ exclusion zone and for 90% C.L., our data are outside this region.

Our analysis pointed out a global best fit with $\chi^2_{\rm min}$/d.o.f. = 2.021/14 and goodness of ≈99.99%, for

$$\begin{aligned} &\delta m^2_{21} = 6.35\text{x}10^{-11}\text{eV}^2 \\ &\delta m^2_{31} = 1.30\text{x}10^{-3}\text{eV}^2 \\ &\sin^2(2\omega) = 0.70 \\ &\sin^2(2\phi) = 0.25 \end{aligned} \tag{11}$$

and a local best point with $\chi^2_{\rm min}$/d.o.f = 2.024/14 and goodness of ≈99.99%, for

$$\begin{aligned} &\delta m^2_{21} = 1.30\text{x}10^{-11}\text{eV}^2 \\ &\delta m^2_{31} = 6.40\text{x}10^{-4}\text{eV}^2 \\ &\sin^2(2\omega) = 0.37 \\ &\sin^2(2\phi) = 0.61 \end{aligned} \tag{12}$$

$\sin^2(2\omega)$	$\sin^2(2\phi)$	δm^2_{21} (eV^2)	δm^2_{31} (eV^2)	C.L. (%)
0.29-0.53	0.58-0.65	1.15-1.40 x 10^{-10}	4.85-7.10 x 10^{-4}	
0.68-0.78	0.19-0.23	4.90-7.25 x 10^{-11}	1.15-1.45 x 10^{-3}	90
0.28-0.61	0.57-0.71	1.10-1.45 x 10^{-10}	4.25-7.25 x 10^{-4}	
0.67-0.90	0.18-0.36	4.15-7.40 x 10^{-11}	1.10-1.45 x 10^{-3}	95
0.25-1	0.56-0.95	1.05-1.45 x 10^{-10}	3.25-7.25 x 10^{-4}	
0.62-1	0.16-0.39	3.65-7.50 x 10^{-11}	1.05-1.45 x 10^{-3}	99

Table 1
Limits for the values of the mixing angles and mass parameters.

These points have almost the same precision and were placed on the plots of figure 1 and in the figure 2.

To test if the choice of X_{31} smaller than X_{21} gives a better result than putting it at the same order of the latter we made the calculation of the allowed regions for the parameters δm^2_{21}, $\sin^2(2\omega)$ and $\sin^2(2\phi)$, with the δm^2_{31} "non-dependence". Our results are shown in the figures 3(a) and (b), where we have again the parameter δm^2_{21} within the expected limits. We found a best point with $\chi^2_{\min}$/d.o.f = 6.39/15 and goodness of 97.25%, for

$$\begin{aligned} &\delta m^2_{21} = 6.35\text{x}10^{-11}\text{eV}^2 \\ &\sin^2(2\omega) = 0.48 \\ &\sin^2(2\phi) = 0.99 \end{aligned} \tag{13}$$

In the figure 4(a) we see the full and dotted lines representing, respectively, the suppression rates with recoil-e^- spectrum as a function of the energy, for the global and local best values, calculated with the dependence on δm^2_{31} and for the dashed line we see the same calculation for the "non-dependence" on that parameter, where we average the argument in $\sin^2(\frac{\delta m^2_{31} X_{31}(t)}{4\hbar c E})$ to $\frac{1}{2}$ as explained on section 2. We can observe that the two first curves are very close to the experimental points, giving a good agreement for the low energy spectrum and a satisfactory explanation for the high energy excess, providing a better result than the third curve.

In figure 4(b) we compare our results with the suppression rate obtained for the experimental data divided by the SSM estimated flux. We made the calculation for 8 time bins of 1.5 months each, which cover all data points, for $E_\nu > 11.5$ MeV. Our best result with $\delta^2_{m_{31}}$ dependence is represented by the full line for the values

$$\delta m^2_{21} = 1.08\text{x}10^{-10}\text{eV}^2$$

$$\delta m^2_{31} = 4.99\text{x}10^{-4}\text{eV}^2$$
$$\sin^2(2\omega) = 0.57$$
$$\sin^2(2\phi) = 0.64 \qquad (14)$$

with χ^2_{min}/d.o.f. = 1.18/4 and goodness of 88.11%, what gives a result better than the analysis with $\delta^2_{\text{m}_{31}}$ "non-dependence" as seen bellow

$$\delta m^2_{21} = 7.75\text{x}10^{-11}\text{eV}^2$$
$$\sin^2(2\omega) = 0.53$$
$$\sin^2(2\phi) = 0.99 \qquad (15)$$

with χ^2_{min}/d.o.f. = 3.30/5 and goodness of 65.45%. The suppression rate for this point is illustrated by the dashed line in the figure 4(b). The dotted line in the same figure is the suppression rate calculated for the seasonal variation in the absence of neutrino oscillations, modulated by the orbital eccentricity of the Earth,

$$\text{R}^{\text{seas}} = \text{R}^{\text{S-K}}(1 - \xi cos(2\pi t))^{-2} \qquad (16)$$

where $\text{R}^{\text{S-K}} = 0.465 \pm 0.005\ ^{+0.015}_{-0.013}$ [5] and ξ is the eccentricity of the Earth (0.0167) with t running over one year. The suppression rate with no oscillations for the 1117 days data has χ^2_{min}/d.o.f. = 4.1/7 with 76% of goodness, which is in agreement with the data despite of our $\delta^2_{\text{m}_{31}}$ dependence analysis provide a better value, what remains not conclusive for the validity of the vacuum oscillation solution for the solar neutrino problem reaffirming the need for detectors sensitive to the monoenergetic ^{7}Be neutrinos which are more influenced by the seasonal variation than the ^{8}B neutrino flux.

5 Conclusions

We show that the Super-Kamiokande solar neutrino data is better explained in a three-neutrino vacuum oscillation scenario, with the mass parameters ranging from 3.65 x 10^{-11} to 1.45 x 10^{-10} eV^2 and 3.25 x 10^{-4} to 1.45 x 10^{-3} eV^2 for $\delta^2_{\text{m}_{21}}$ and $\delta^2_{\text{m}_{31}}$, respectively, by the differentiation of the oscillation lenght for $\nu_e \overrightarrow{\leftarrow} \nu_\mu$ from that one for $\nu_e \overrightarrow{\leftarrow} \nu_\tau$. This procedure also gives a good fit for the seasonal variation of the data with $\text{E}_\nu > 11.5$ MeV.

The choice of the distance X_{31} for solar neutrinos on the same order of the atmospheric neutrinos and assuming that the atmospheric neutrino anomaly can be explained with two flavour oscillations ($\nu_\mu \overrightarrow{\leftarrow} \nu_\tau$) in vacuum, turns feasi-

ble a unification of the solar neutrino vacuum oscillations solution with that one for atmospheric neutrinos.

The accumulation of data from Super-Kamiokande seems to indicate a statistical origin for the excess of events around 13.0 MeV, since we have a decrease of about 33% in the suppression rates for the data points gathered in the period from 504 to 1117 days of operation. Besides, the good fit obtained in this work, tends to discard solutions using vacuum oscillation with modifications in the neutrino fluxes from the SSM, but a more profound calculation should be made to confirm this assertion.

References

[1] Y. Suzuki, Nucl. Phys. B (Proc. Suppl.) 77 (1999) 35.

[2] Y. Totsuka, Symp. on Relat. Astrophysics (Paris, December 1998).

[3] K. Inoue, Talk at the 8th Int. Workshop "Neutrino telescopes" (Venice, February 1999).

[4] Y. Suzuki, Talk at the XIX Symp. on Lepton and Photon Interactions at High Energies (Stanford University, August 1999).

[5] Y. Suzuki, Talk at the XIX Int. Conf. on Neutrino Physics and Astrophysics (Sudbury, June 2000).

[6] J.N. Bahcall *et al.*, Phys. Lett. B 433 (1998) 1; J.N. Bahcall *et al.*, Phys. Rev. D 58 (1998) 096016.

[7] J.N. Bahcall and P.I Krastev, Phys. Lett. B 436 (1998) 243.

[8] R. Escribano *et al.*, Phys. Lett. B 444 (1998) 397.

[9] P.I. Krastev and S.T. Petcov, CERN preprint CERN-TH 6401/92 (1992).

[10] CHOOZ Collaboration, M. Apollonio *et al.*, Phys. Lett. B 420 (1998) 397; *ibid* 466 (1999) 415.

[11] C. Arpesella *et al.*, Borexino proposal, Vols. 1 and 2; (G.Bellini *et al.*, University of Milano, Milano, 1992); R.S. Raghavan, Science 267 (1995) 45.

[12] A. Suzuki (for the KamLAND Collaboration), Nucl. Phys B (Proc. Suppl.) 77 (1999) 171.

[13] V. Barger *et al.*, Phys. Rev. Lett. 93B (1980) 194; G.L. Fogli *et al.*, Phys. Rev. D 49 (1994) 3626.

[14] V. Barger *et al.*, Phys. Rev. D 43 (1991) 1110.

[15] T.K. Gaisser, Cosmic rays and particle physics (Cambridge Univ. Press, Cambridge, 1990).

[16] T.K. Kuo and J. Pantaleone, Rev. Mod. Phys. 61 (1989) 937; G.L. Fogli *et al.*, Phys. Rev. D 49 (1994) 3626; V. Barger and K. Whisnant, Phys. Rev. D 59 (1999) 093007.

[17] J.N. Bahcall, Rev. of Mod. Physics 59 (1987) 505; J.N. Bahcall *et al.*, Phys. Rev. D 51 (1995) 6146; Phys. Rev. C 55 (1997) 494; B. Faïd *et al.*, Phys. Rev. D 55 (1997) 1353; Astrop. Phys. 10 (1999) 93.

[18] M.C. Gonzales-Garcia *et al.*, Nucl. Phys. B 573 (2000) 3.

Acknowledgements

We would like to thank the CNPq (Conselho Nacional de Desenvolvimento Científico e Tecnológico) for the financial support and the CBPF (Centro Brasileiro de Pesquisas Físicas) for the facilities.

List of Figures

Figure 1 - Projections in six phase spaces of the allowed regions for the mixing angles and mass parameters. The regions are calculated with 99% (outer area), 95% (intermediate area) and 90% C.L.(inner area). • represents the global best fit and ⋄ the local best fit.

Figure 2 - Comparison of the figure 1(e) with the CHOOZ Collaboration results. The regions are calculated with 99% (outer area), 95% (intermediate area) and 90% C.L. (inner area). • represents the global best fit and ⋄ the local best fit.

Figure 3 - Allowed regions for the mixing angles and the mass parameter $\delta^2_{m_{21}}$ with $\delta^2_{m_{31}}$ "non-dependence". The regions are calculated with 99% (outer area), 95% (intermediate area) and 90% C.L. (inner area). • represents the best fit point.

Figure 4 - Comparison of our results with the ratio of the measured to the calculated number of events with recoil-e^- energy (a) and the 1.5 months binned seasonal variation data for $E_\nu > 11.5$ MeV (b). In (a) the full and dotted lines represent, respectively, the calculated suppression rates via neutrino oscillations in vacuum for the global and local best fit point with $\delta^2_{m_{31}}$ dependence and the dashed line is the same with $\delta^2_{m_{31}}$ "non-dependence". In (b) the full line represents the calculated rates for the best fit point with $\delta^2_{m_{31}}$ dependence and the dashed line the best fit point with $\delta^2_{m_{31}}$ "non-dependence". The dotted line is the expected seasonal variation due to the Earth eccentricity without neutrino oscillations.

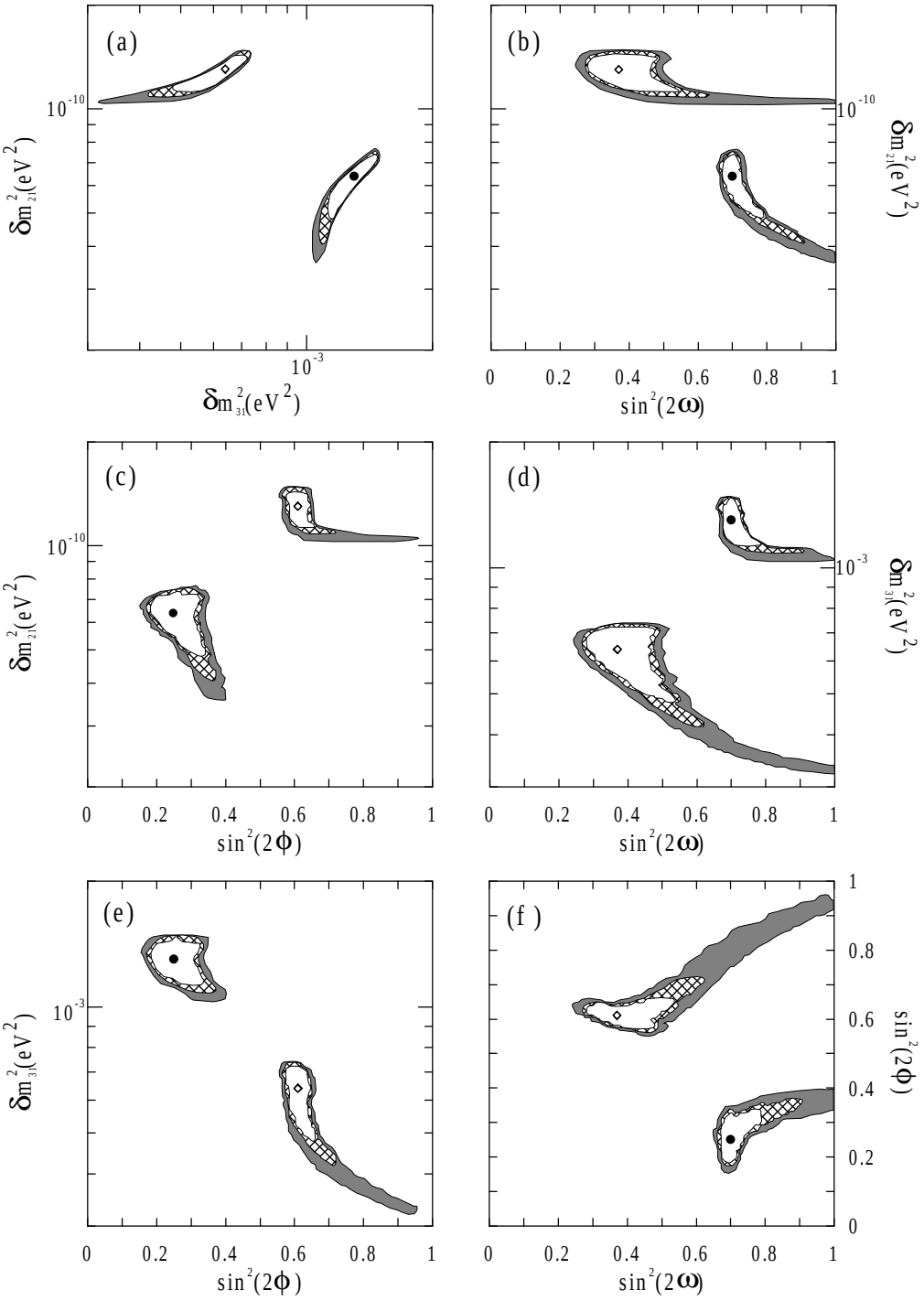
(a)
(b)
(c)
(d)
(e)
(f)
10^{-10}
10^{-3}
$\delta m^2_{21}(eV^2)$
$\delta m^2_{31}(eV^2)$
$\sin^2(2\omega)$
$\sin^2(2\phi)$
0
0.2
0.4
0.6
0.8
1

Figure 1

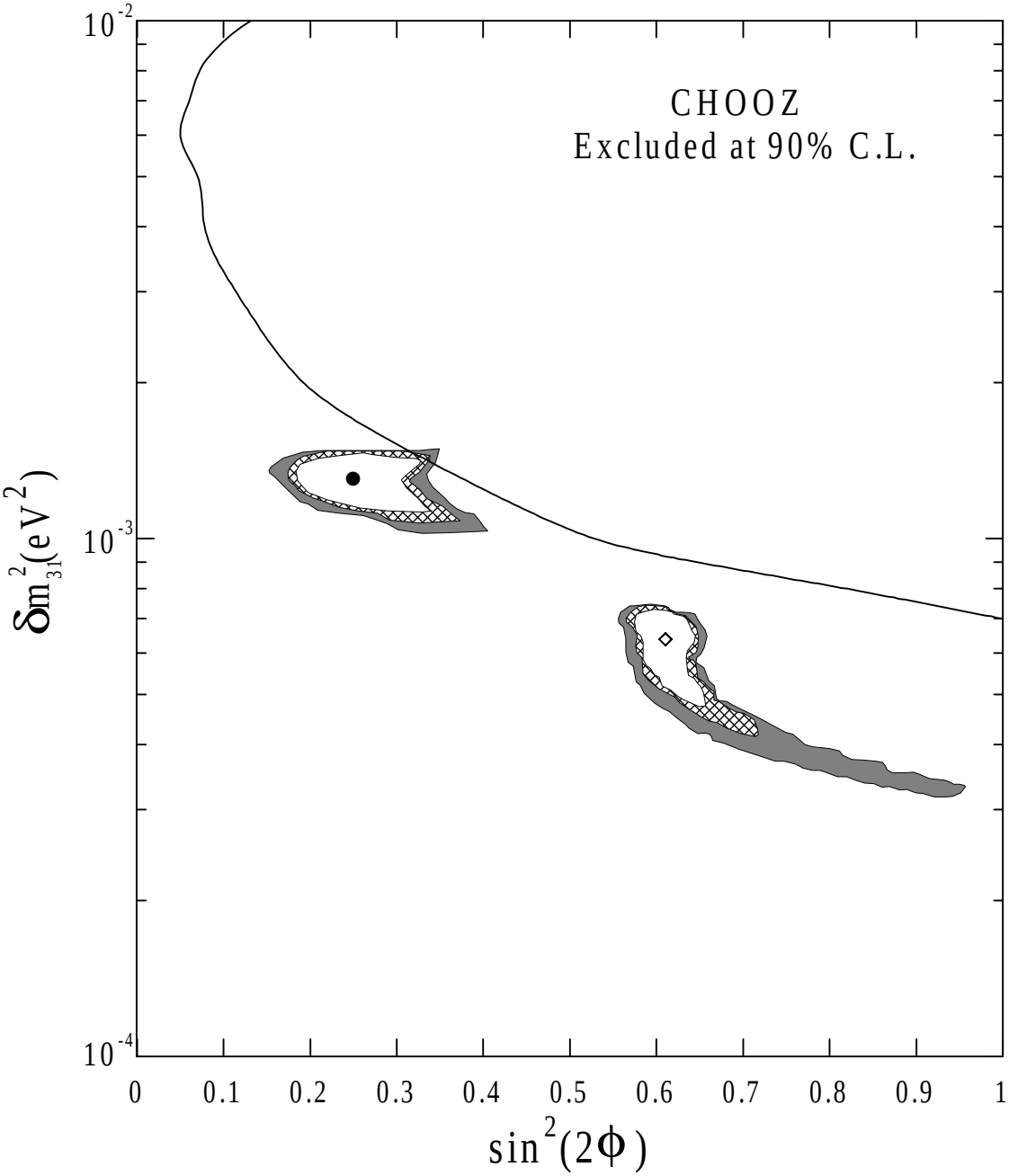
CHOOZ
Excluded at 90% C.L.
10^{-2}
10^{-3}
10^{-4}
$\delta m^2_{31}(eV^2)$
0
0.1
0.2
0.3
0.4
0.5
0.6
0.7
0.8
0.9
1
$\sin^2(2\Phi)$

Figure 2

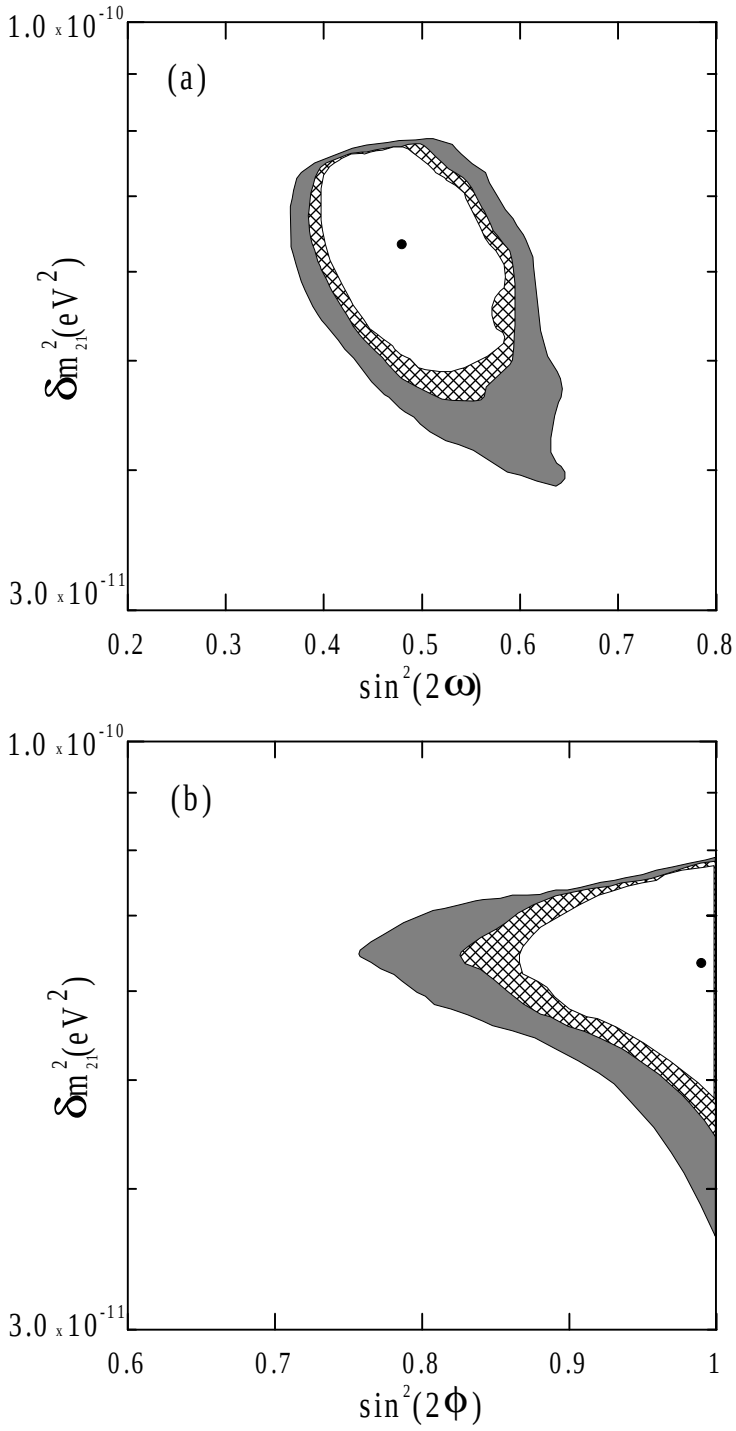
(a)
1.0 x 10^-10
3.0 x 10^-11
δm^2_21(eV^2)
0.2
0.3
0.4
0.5
0.6
0.7
0.8
sin^2(2ω)
(b)
1.0 x 10^-10
3.0 x 10^-11
δm^2_21(eV^2)
0.6
0.7
0.8
0.9
1
sin^2(2φ)

Figure 3

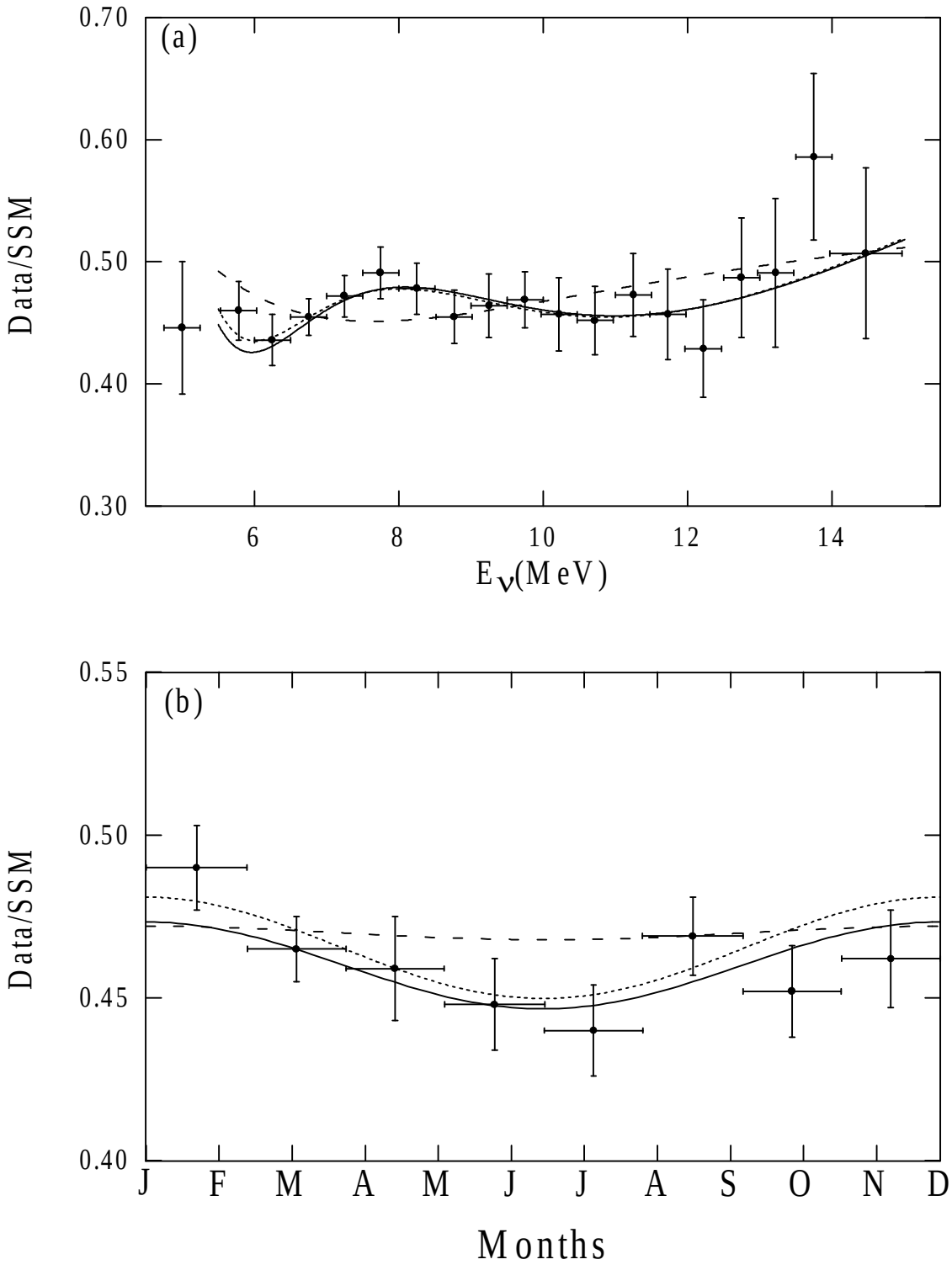
(a)
0.70
0.60
0.50
0.40
0.30
Data/SSM
6
8
10
12
14
E_ν(MeV)
(b)
0.55
0.50
0.45
0.40
Data/SSM
J F M A M J J A S O N D
Months

Figure 4